Cilt 12, Sayı 1, Sayfa 153-162, 2023 Volume 12, Issue 1, Page 153-162, 2023

Araştırma Makalesi https://doi.org/10.46810/tdfd.1205088 Research Article

Türk Doğa ve Fen Dergisi
Turkish Journal of Nature and Science
www.dergipark.gov.tr/tdfd

Investigation of the Magnetic and Mechanical Properties of Nano-Y2O3 Doped Bismuth Based Superconductor Materials

Emine Burcu CEVİZCİ [1*], Kemal KOCABAŞ[1], Sedat KURNAZ[2]

[1] Dokuz Eylul University, Science Faculty, Physics Department, İzmir, Türkiye
[2] Kastamonu University, Central Research Laboratory, Kastamonu, Türkiye
Emine Burcu CEVİZCİ ORCID No: 0000-0002-1738-4130
Kemal KOCABAŞ ORCID No: 0000-0002-4443-0059
Sedat KURNAZ ORCID No: 0000-0003-3657-2628

**Corresponding author: cevizciburcu@gmail.com*

(Received: 15.11.2022, Accepted: 14.03.2023, Online Publication: 27.03.2023)

Keywords
nano- Y_2O_3, BSSCO, Critical Current Density, Hole concentration, Microhardnes

Abstract: The effects of nano-Y_2O_3 addition on the structural, superconducting, magnetic and mechanical properties of Bi-2223 superconducting system were investigated in this study. Bulk polycrystalline samples with general formula of $Bi_{1.8}Pb_{0.4}Sr_2Ca_2Cu_3O_{10+\delta}$ + (Y_2O_3) with (x; weighted % 0.0-0.2-0.4-0.8-1.0) were prepared by solid state reaction method. X-ray diffraction (XRD), Scanning Electron microscope (SEM), Energy dispersive X-ray spectroscopy (EDX) measurement, Vibrating sample measurement (VSM), Resistance- temperature (ρ-T) measurement and Vickers microhardness measurement (VHM) were also used for samples structural characterizations. XRD patterns showed that both Bi -2223 and Bi-2212 phases are coexist in the samples. While a lattice parameter increased, c lattice parameter decreased with increasing nano- Y_2O_3 addition. In SEM photographs, it is seen that granular structure is plate-like in all samples. The presence of point particles on the layered particles has been seen more clearly with increasing Y_2O_3 addition. Hole concentration values that calculated from ρ-T measurement, ranges from 0.113 to 0.160. While amount of Y2O3 addition increased, critical transition temperatures decreased. VSM results showed that critical current density values increase with Y2O3 addition. VHM results showed that the hardness value increased until x= 0.4% additive sample and decreased after this value.

Nano-Y2O3 Katkılı Bizmut Esaslı Süperiletken Malzemelerin Manyetik ve Mekanik Özelliklerinin İncelenmesi

Anahtar Kelimeler
nano- Y2O3, BSSCO, Kritik Akım Yoğunluğu, Delik konsantrasyon, Mikrosertlik

Öz: Bu çalışmada nano-Y_2O_3 ilavesinin Bi-2223 süperiletken sisteminin yapısal, süperiletken, manyetik ve mekanik özellikleri üzerindeki etkileri araştırılmıştır. Bi1.8Pb0.4Sr2Ca 2Cu3O10 + δ + (Y_2O_3) ile (x; ağırlıkça % 0,0-0,2-0,4-0,8-1,0) genel formülüne sahip polikristal örnekler katıhal reaksiyon yöntemiyle hazırlandı. Örneklerin yapısal karakterizasyonları için X-ışını kırınımı (XRD), Taramalı Elektron mikroskobu (SEM), Enerji dağılımlı X-ışını spektroskopisi (EDX) ölçümü, Titreşimli numune ölçümü (VSM), Direnç-sıcaklık (ρ-T) ölçümü ve Vickers mikrosertlik ölçümü (VHM) yapılmıştır. XRD desenleri, örneklerde hem Bi -2223 hem de Bi-2212 fazlarının bir arada bulunduğunu gösterdi. Nano-Y ilavesinin artmasıyla a örgü parametresi artarken, c örgü parametresi azalmıştır. SEM fotoğraflarında tüm örneklerde tanecik yapısının plaka benzeri olduğu görülmekte ve katkı miktarındaki artmasıyla tabakalı yapı üzerinde nokta şeklinde partiküllerin varlığı daha net görülmektedir. ρ-T ölçümünden hesaplanan delik konsantrasyonu değerleri 0,113 ile 0,160 arasında değişmektedir. Nano-Y miktarı artarken kritik geçiş sıcaklıkları azalmıştır. VSM sonuçları Nano-Y eklenmesiyle kritik akım yoğunluğu değerlerinin arttığını göstermektedir. VHM sonuçları, sertlik değerinin x= % 0,4 katkılı örneğe kadar arttığını ve bu değerden sonra azaldığını göstermiştir.

1. INTRODUCTION

Superconducting materials are sometimes used as high-field magnets to store large amounts of energy. Therefore, superconductivity must persist up to high magnetic fields. High temperature superconductors have two critical field values: the lower critical (H_{c1}) and the upper critical magnetic (H_{c2}) field. When applied magnetic field (H) intensity is $H_{c1}<H<H_{c2}$, the magnetic field penetrates the superconductor and the superconductivity state is destroyed locally around a vortex [1]. Therefore, the superconducting state and the normal state coexist (mixed state). If the superconductor in the mixed state carries a carrying current, the electrons in the flux lines are exposed to the electromotive force depending on the direction of the magnetic field and the current. Electrons moving under the influence of this force cause ohmic losses. It is possible to eliminate these losses by preventing movement of the flux lines. Flux fixation is provided by various defects in the samples, such as impurities, dislocations, normal precipitates, voids, and grain boundaries. These impurities and defects are called needling centers. In this way, superconducting materials can maintain their superconductivity even at higher magnetic field values.

The critical current density J_c can be increased by the formation of artificial active needling centers as they can prevent the movement of flux lines causing flux shift. Since dimensions of nano-sized particles are closer to the coherent length in relation to the characteristic Cooper pair size, nano doping in Type II superconductors can create stronger needling force in magnetic flux stabilization. The addition of nanoparticles to Bi-2223 superconducting phase plays an important role in flux stabilization and increasing critical current density [2]. Flux stabilization is due to nanoparticles being trapped inside the superconducting grains and producing crystal defects within superconducting particles by creating secondary phase defects [3]. For this reason, many studies have been carried out in the literature on the incorporation of different nano-sized elements into the BSCCO system. It is seen that some nanodopings, such as nano-Au [4], nano-Ag [5], nano-PbO–CdO composite [6], nano-ZrO_2 [7] and nano-Sn [8], improve the transport and superconduting properties of the system. The powders in the chemical composition of BiSrCaCuO (BSCCO), a Type II superconductor, have low toxicity. The high thermodynamic stability of the components of this material enables formation of high critical temperature (T_c) phases more easily [4]. Because of these properties, they are useful materials in terms of technological applications in order to increase cost efficiency in electricity consumption and to provide lossless power transfer. By improving the superconductivity, magnetic and mechanical properties of the system, it will increase the possibilities of use in industrial and medical applications.

In literature, it is seen that studies have been carried out on the improvement of the superconductivity and mechanical properties of Bi-2223 superconducting materials with micro-scale Y_2O_3 doping. In these studies, it is seen that the system improves the superconductivity and mechanical properties [9-12]. Suazlina et al. [13], reported the effects of Y_2O_3 nano particle addition in Bi-2212 superconductors. It was found that critical temperature and critical current density increased up to x=0.7 wt%. Again, in a study conducted by Oboudi in 2016 [14], nano Y_2O_3 was added to $Bi_{1,8}Pb_{0,4}Sr_2Ca_2Cu_3O_{10+y}$ superconductor samples with different weight percentages. As the additive ratio increased, the current density increased by 200% and superconductivity transition temperature increased by 3%. In both studies, it is seen that both critical temperature and critical current density values of BSCCO system with Y_2O_3 addittion increased. In our study, it is aimed to synthesize $Bi_{1,8}Pb_{0.3}Sr_2Ca_2Cu_3O_y$ superconducting ceramics by doping nano-Y_2O_3 with different weight percentages in order to improve the magnetic and mechanical properties of the obtained samples.

2. MATERIAL AND METHOD

$Bi_{1.8}Pb_{0.3}Sr_2Ca_2Cu_3O_y$ superconducting samples were synthesized using a solid state reaction method. In the first step of the synthesis process, Y_2O_3 nanoparticles were added by small weight percentages (x=0.2, 0.4, 0.6, 0.8, and 1.0 wt %). Stoichiometric amounts of starting high-purity (≥99.99%) Bi_2O_3, PbO, $SrCO_3$, $CaCO_3$, CuO (15–45 nm) and nanosized Y_2O_3 (18-38 nm) powders were thoroughly mixed. **Figure 1** has been given a schematic representation of the experimental process.

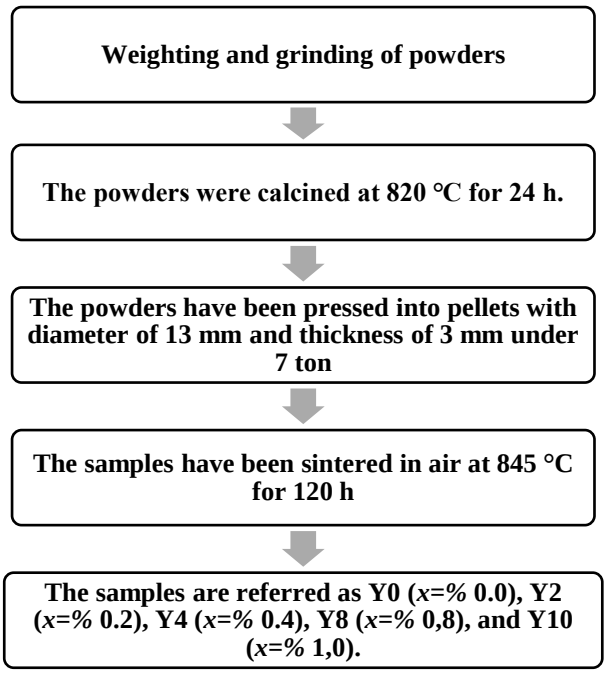

Figure 1. Experimental Procedure

The lattice parameters, the phase purity, crystal structure and grain size of samples were obtained from XRD. Phase analysis of the samples was determined with the help of X-PowderX program. The grain structure and surface morphology of the samples were examined with 10000x magnification by scanning electron microscope (SEM) photographs. Energy-dispersive spectrometry

(EDS) was applied for the elemental analysis of the samples. Magnetization curves of the samples depending on the magnetic field strength were taken with Vibrating Sample Magnetometer (VSM) measurements. Critical current density calculations of samples were made with the data obtained from the M-H curves and Bean Model [15]. Microhardness measurements of the samples were made with the Mitutoyo digital microhardness tester of the *HM-200* series.

3. RESULTS

The phase purity, the lattice parameters and crystal structure of samples were obtained from XRD patterns. XRD scans were made with CuK_α radiation between 3° to 70°. The wavelength used is λ=0.15406 nm. X-ray patterns of nano-Y_2O_3 addition samples are shown in **Figure 2.** In the XRD patterns, The peaks of Bi-2223 phase are labeled with open circle, the peaks of the Bi-2212 phase are labeled with filled circle, and the peaks of the Ca_2PbO_4 phase are labeled with filled diamond. XRD patterns showed that the majority phase consisted of Bi-2223 and Bi-2212 phases in all samples [16]. Impurity phase Ca_2PbO_4, which is accelerating the formation of the Bi-2223 phase, was observed at very low peak intensity at 2θ=17.80° in all samples except Y0 and Y2 samples [17]. No peaks of Y_2O_3 nanoparticles were found in the XRD model. This result showed that nano-Y_2O_3 addition did not enter the crystal structure. This may be due to the very small amount of additives made. The volume fraction and the lattice parameters of the samples are listed in **Table 1**.

Table 1. Lattice parameters and volume fraction of $Bi_{1.8}Pb_{0.4}Sr_2Ca_2Cu_3O_{10+\delta}$ + (Y_2O_3) samples

Nano Y_2O_3	a (Å)	b (Å)	c (Å)	Volume Fraction (Bi-2223/Bi-2212)
Y0	5.339	5.3995	37.0740	66.11/33.89
Y2	5.3488	5.3858	36.9768	63.92/36.08
Y4	5.3450	5.4081	36.8568	63.04/36.96
Y8	5.3488	5.3642	36.7716	59.02/40.98
Y10	5.3412	5.3764	36.7596	58.68/41.31

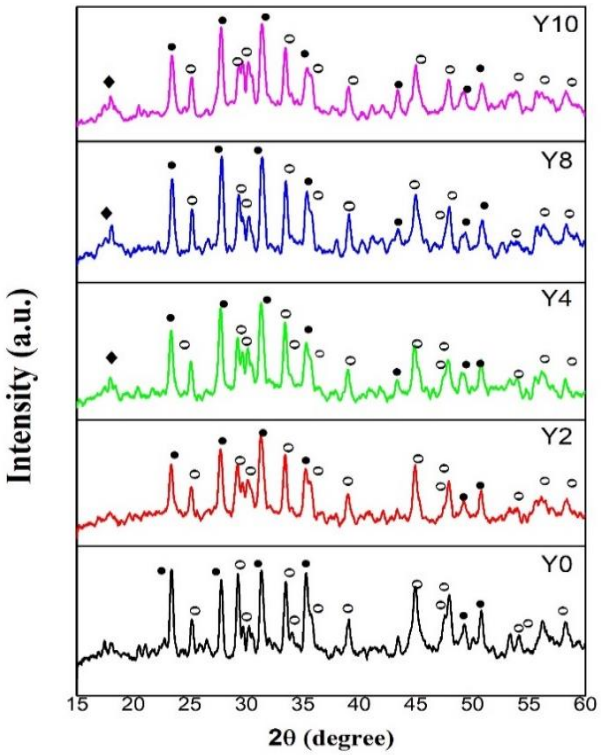

Figure 2. X-ray diffractometers at room temperature for the $Bi_{1.8}Pb_{0.4}Sr_2Ca_2Cu_3O_{10+\delta}$ + (Y_2O_3) with (x; weighted % 0.0-0.2-0.4-0.8-1.0) , open circle Bi-2223 phase, filled circle Bi-2212 phase, filled diamond Ca_2PbO_4.

The volume ratio of Bi-2223 and Bi-2212 phases was calculated according to the equations below using the intensities of the peaks [18]:

$$Bi-[2223](\%) = \frac{\sum I\,(2223)}{\sum I(2223)+\sum I(2212)} x100 \quad (1)$$

$$Bi-[2212](\%) = \frac{\sum I\,(2212)}{\sum I(2223)+\sum I(2212)} x100 \quad (2)$$

where I_{2223} and I_{2212} are the intensities of the XRD peaks for Bi-2223 and Bi-2212 phases, respectively. It was observed that the percentage of Bi-2212 phase increases and the percentage of Bi-2223 phase decreases with increasing addition of nano- Y. We observed that the decrease in the volume fraction of the Bi-2223 phase in all doped samples was quite small [23]. These results showed that small amounts of nano-Y_2O_3 addition effectively contribute to the phase stability of BSCCO systems. Doping material slightly affected the low T_c phase (Bi-2212) and high Tc phase (Bi-2223) ratios [19]. The cell parameters of all samples showed that the Bi-2223 phase is dominant. According to the calculated lattice parameters, the crystal lattice of all samples was found to be orthorhombic.

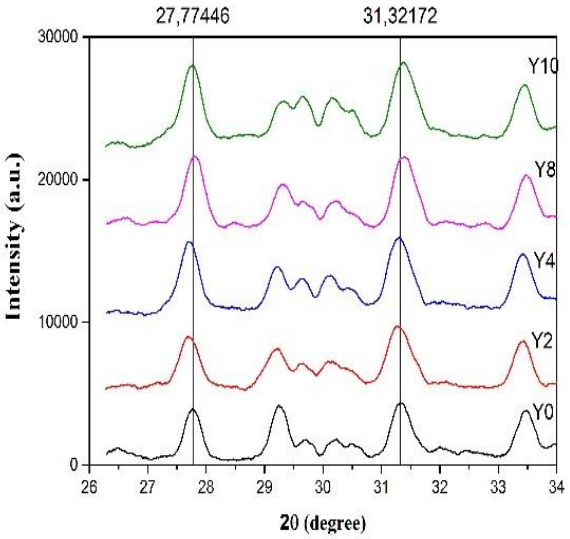

Figure 3. The peak shift of the strongest peaks due to the Y_2O_3 doping.

Figure 3 has been showed that peak shift of the strongest peaks.Right and left shifts in the angle of the peaks are caused by point or dislocation defects, stress and strains that occur during the synthesis process. Defects in the structure cause the width of the peaks to increase, while the distortions in the lattice affect the peak positions. Shift in peak towards right is an indication of orthorhombic crystal formation tending the sample to attain superconducting state. When we looked at the positions of the peaks, we did not see that there is no significant peak shift. Accordingly, the orthorhombic structure continues to exist in all samples.

Table 2. Grain size, Critical current density and Critical temperature of $Bi_{1.8}Pb_{0.4}Sr_2Ca_2Cu_3O_{10+\delta}$ + (Y_2O_3) samples

Nano Y_2O_3	Grain size (nm)	Dislocation density δ (nm-2)	*Jc (0)*	*Tc*(on set) (Kelvin)
Y0	49.88	0.000401	164.15	105
Y2	30.51	0.001074	211.11	109
Y4	30.39	0.001082	232.73	110
Y8	53.64	0.000347	177.96	75
Y10	35.08	0.000812	120.88	90

In **Table 1**, it is seen that there is no change the volume fraction of the 2223-phase in nano-Y_2O_3 addition samples compared to the undoped sample [14]. The nano-Y_2O_3 addition has been effectively added to the phase stability of the BSCCO systems. While parameters a and b did not change, a small decrease occurred in parameter c in nano-Y doped samples (**Figure 4**).
The reason for the small change in the c lattice parameter:

1. We think that the reason for the small change in the c parameter is due to the change in the hole concentration in the CuO_2 planes. The doped ions may change the spacing between CuO layers, afecting the charge transfer to CuO layers. The hole transfer from Cu planes to Bi–O bonds leads to the contraction of Bi–O layers, causing a decrease in c-axis [20].

2. The lattice distortions that manifest themselves in the formation of the modulated structure of the bismuth high temperature superconductors, as a rule, are attributed to the geometric mismatch between the Bi_2O_2 bismuth–oxygen and CuO_2 copper–oxygen blocks [21].

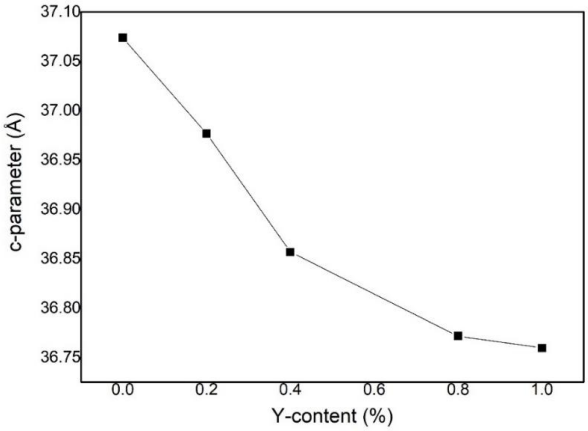

Figure 4. Variation of *c*-lattice parameters with nano-Y additive for Bi (Pb):2223 samples.

Grain size of the samples can be determined from XRD patterns using Scherrer Formula which is shown in Eq. (3) [22].

$$D = \frac{K\lambda}{B\cos(\theta)} \quad (3)$$

Here *D* is the mean size of grain, *B* is the line broadening at half the maximum intensity (FWHM) in radians, λ= 0.15406 nm is the X-ray wavelength and θ is the Bragg angle. K is Scherrer constant which depends on the crystallite shape and size distribution, indices of the diffraction line [23]. The value of the *K* constant, which ranges from 0.62 to 2.08, can be affected by microstrain in the crystal. In our study, we accepted *K* = 0.94 and the calculated values of *D* represent estimates. The Y4 sample has the smallest particle size and Y8 has the biggest particle size. This may be related to the grinding step of the samples during the preparation process. The particle sizes calculated from the XRD results and the particle development seen from the SEM photographs are similar.

In order to characterize the microstructure of the samples, SEM and EDX analyzes were made and the distribution of the elements in the structure was examined. EDX was used to confirm their chemical composition. SEM microscope images were taken and their morphologies and particle sizes were examined. In **Figure 5 (a-e)**, it is clearly seen that the structure is in a stratified form. This type of configuration is the general structure of the BSCCO system. It is observed that the layered structure continues to exist with increasing nano-Y_2O_3 addition. As from Y2 sample, while the layered structure still exists, the existence of agglomeration of small particles on the layered structures draws attention. With the increase in the amount of additive, the presence

of point particles on the layered particles is seen more clearly. This result can be thought to play a role in the formation of artificial needling centers on the samples due to the fact that the nano-dopeds could not enter the structure, but were trapped inside the superconductor grains, revealing the secondary phase defects and producing crystal defects in the superconducting particles [24]. It is thought that the black voids that occur in some places are considered as non-superconducting regions and that they are formed as a result of breaking the connections between the particles. when examined all SEM photos, It has been seen that with increasing nano-Y_2O_3 addition, the voids on the surface of the samples increase and cracks occur on the sample surface. The SEM results are well supported by the XRD results. In addition to the intergranular distribution of nanoparticles, the presence of nanoparticles can be observed in other parts of the microstructure of nano-Y_2O_3 addition samples. A increase in grain size was observed for Y8 and Y10 samples, which could reduce the superconductivity properties of the BSCCO system.

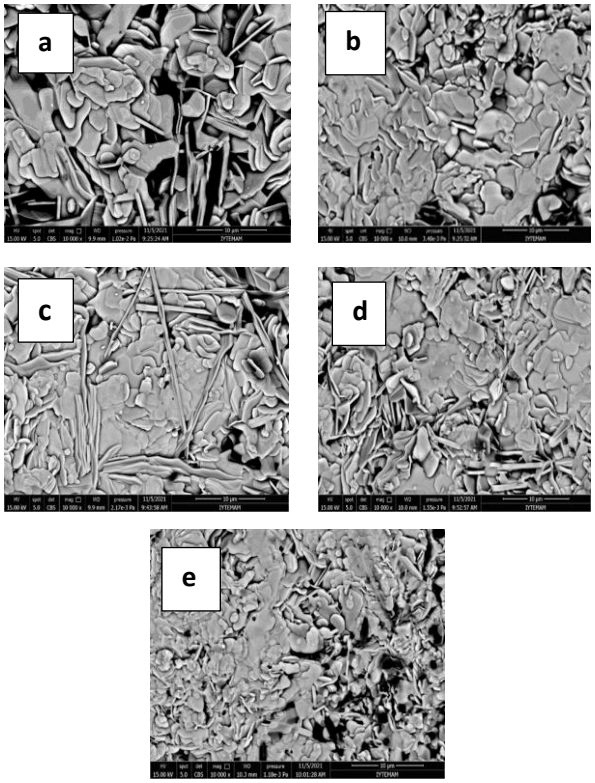

Figure 5. SEM images of **a** Y0, **b** Y2, **c** Y4, **d** Y8, and **e** Y10 samples.

According to the results of EDX elemental analysis in **Figure 6 (a-e)**, increase in the additive ratios (%) and the oxygen (O), Bismuth (Bi), Lead (Pb), Strontium (Sr), Calcium (Ca) and Copper (Cu) ratios (%) values in the samples did not change much. The EDX analysis results showed that element percentages are mostly in the desired composition for the prepared superconductor samples. The amount of Y on the sample surfacehas been increased with increasing nano-Y addition. The analysis on sample surface made at different points showed that Y elements in the doped samples are homogeneously distributed throughout the material as expected. In addition, there is no impurity formation in the material. Based on these facts, we can clearly state that the nano-Y_2O_3 element is evenly distributed in the structure.

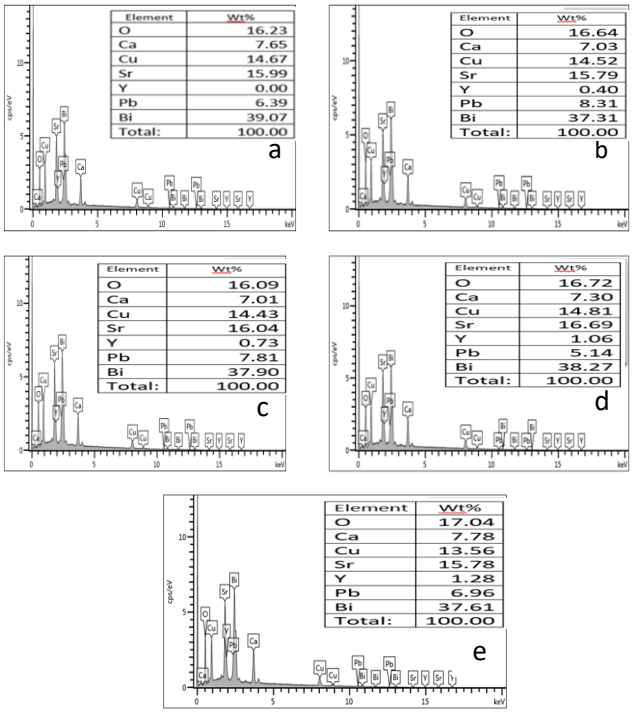

Figure 6. EDX graphs of **a** Y0, **b** Y2, **c** Y4, **d** Y8, and **e** Y10 samples

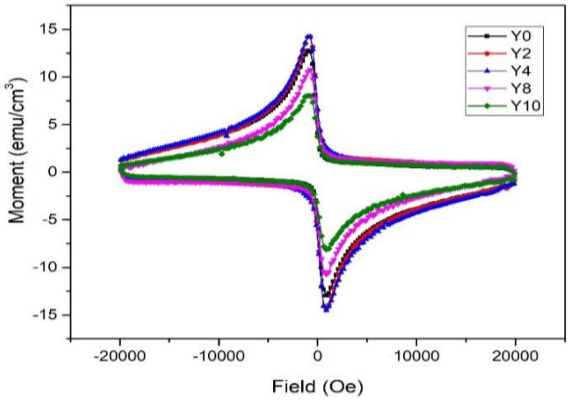

Figure 7. M-H graphs of Y0, Y2, Y4, Y8 and Y10 samples.

The magnetic moment responses of the samples against the external magnetic field applied to the samples were determined by M-H measurement with the VSM method. The obtained samples were subjected to M-H measurement with the Lake Shore VSM device at a temperature of 15 K, under a magnetic field between -20000 Oe and 20000 Oe. When the M-H curves of the samples are examined **(Figure 7)**, a hysteristic characteristic of diamagnetic properties of all samples is observed. For example, the magnetization curve is shaped as a loop, indicating presence of pinning centers on the surface of the material. According to the applied magnetic field, the magnetization values of the samples are listed as Y4, Y0, Y2, Y8 and Y10 from the largest to the smallest. No break was observed in the curves of the samples. This means that the impurity phases present in the structure are not evident. The magnetic values of all

samples decreased with the applied magnetic field exceeding 0 Oe. This situation is interpreted as the result of the decrease in the bond between the particles as a result of the agglomeration of the sample itself.

The magnetic field dependence of J_c was calculated by using the experimental Bean model shown in Equation (4).

$$j_c = 20 \cdot \frac{\Delta M}{a\left(1-\frac{a}{3b}\right)} \quad (5)$$

M value in the equation; It is the magnetization value obtained from the M-H curves. ΔM $[\Delta M = (M^+) - (M^-)]$ is the width of the magnetization curve during the decrease and increase of the area in emu/cm^3. M^+ and M^- are the values of positive and negative region band of the magnetic response of samples against the external magnetic, respectively. The values of a and b (a < b) are the dimensions of the rectangular cross section of the sample perpendicular to the applied area in cm [25].

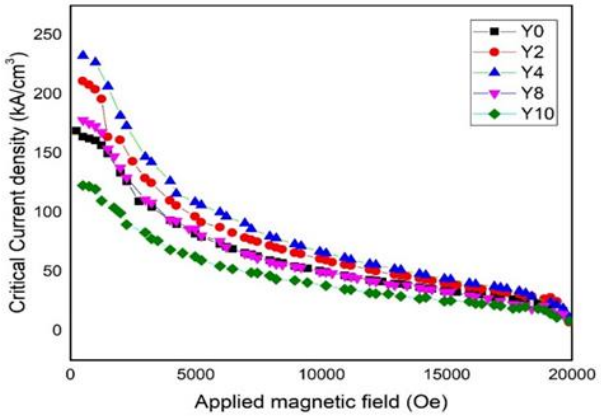

Figure 8. Field dependence of critical current density at 15 K for Y0, Y2, Y4, Y8 and Y10 samples

Figure 8 showed that J_c at 15 K of the samples containing pure and various amounts of nano-sized Y_2O_3. It is clearly seen in the graphs that the *Jc* values of the samples with granular structure decrease as the magnetic field increases. It can be thought that the reason for the decrease in the diamagnetic properties of the samples is due to the weakening of the interparticle bond [26]. In **Table 2**, the highest $J_c(0)$ value for sample Y4 is 232 kA/cm^2. Except for the Y10 sample, the critical current density value of all samples is higher than the undoped sample. Nano-Y_2O_3 addition has a positive contribution to the formation of artificial needling centers. The change in the critical current density depends on the formation of trapping centers in the structure and whether the interparticle bond is intact or not. However, since all of the samples were prepared under the same conditions, considering that the interparticle coupling would be similar in the samples. This irregular change in the critical current density values can only be explained by the increase and decrease in the trapping centers.

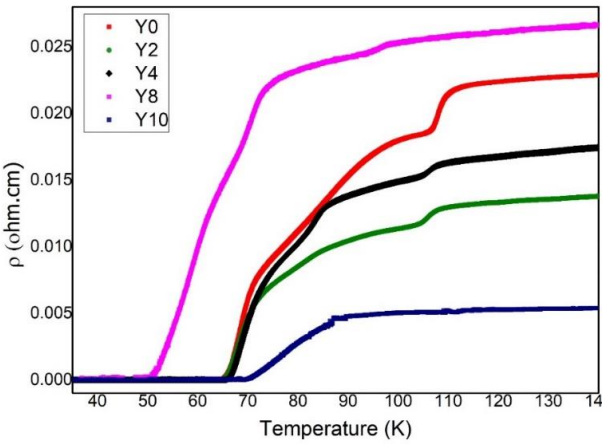

Figure 9. Resistivity temperature graph of Y0, Y2, Y4,Y8 and Y10 samples

Phase transitions that occur in superconducting materials can be determined from the resistivity measurements made depending on the temperature. Resistance temperature measurements were made with DC four probe method between 10 K and 300 K. The resistivity temperature graph of the Bi-based superconductor samples produced in this study is shown in **Figure 9** When the resistivity graph obtained as a function of temperature is examined, it is seen that all samples exhibit metallic behavior in regions above superconductivity transition temperature. With the addition of nano-Y_2O_3 addition in different percentages into the system, superconducting samples exhibit different behaviors in regions below the transition temperature.

$T_{c,onset}$ temperature value is that is the temperature at which the transition from the normal phase to the superconducting phase begins. T_c^{offset} temperature value is the temperature value at which the superconducting phase transition is completed (R=0). The difference between $T_{c,onset}$ and $T_{c,offset}$ temperature values is shown with ΔT_c.

$T_{c,onset}$ temperature value, which gives information about the superconducting phases, was the highest in the Y2 and Y4 sample. As seen in **Table 3**, $T_{c,onset}$ temperature values of Y2 and Y4 samples decrease slightly compared to the undoped sample. However, as the amount of additive increases, we see that the transition temperature to superconductivity decreases considerably. The intergrowth of impurity phases, weak bonding and structural distortions between impurities and superconducting grains can result in a decrease in $T_{c,onset}$ and $T_{c,offset}$ values, as well as an additional increase in the normal state resistivity value. Therefore, our resistivity results showed that the superconducting state was suppressed by increasing nano-Y_2O_3 addition in our system [27].

Table 3. $T_{c,onset}$, $T_{c,offset}$ and Hole concentration values of Y0, Y2, Y4, Y8, and Y10 samples

	$T_{c,onset}$ (K)	$T_{c,offset}$ (K)	ΔT (K)	Hole concentration
Y0	109.5	65	46.36	0.158
Y2	110	65	45.8	0.16
Y4	110	65	45.87	0.16
Y8	98	51	47	0.123
Y10	90	69	21	0.113

Hole concentration values (p) of the samples were calculated by using the following equation proposed by Persland et al [28].

$$p = 0.16 - [(1 - T_c/T^{max}_c)/82.6]^{1/2} \quad (4)$$

where p is the carrier density (numbers of holes); T_c represents the critical temperature values of the samples. T_c^{max} is taken as 110 K for the Bi-2223 system [29].

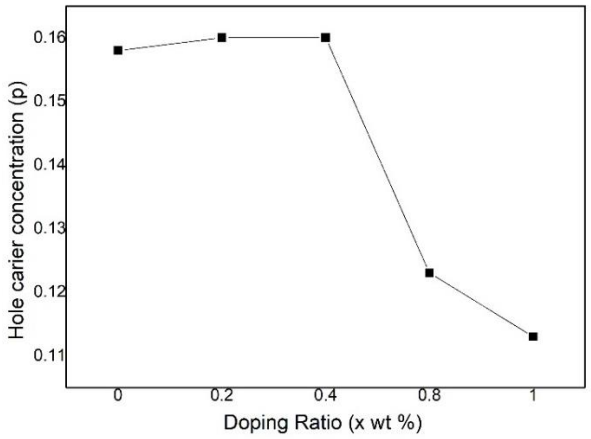

Figure 10. Hole concentration values of undoped and nano-Y_2O_3 added samples

Figure 10 showed that hole carrier concentration values depending on the amount of additive. The hole concentration value ranges from 0.113 to 0.160. Hole concentration values of Y2 and Y4 samples are 0.16. Hole concentration values of Y8 and Y10 samples are 0.123 and 0.113, respectively. It is seen that the carrier density decreases after the value of nano-Y_2O_3 addition x=0.8 %. This result is in agreement with the XRD results. And this result supports our prediction that the decrease in c-parameter seen in XRD results may be due to the decrease in hole concentration [30].

$$H_v = 1854.4\left(\frac{F}{d^2}\right) \quad (GPa) \quad (5)$$

Vickers microhardness was calculated using the equation (5) given above [31]. The applied load is F (N) and d is the average diagonal length of the indentation impression (μm).

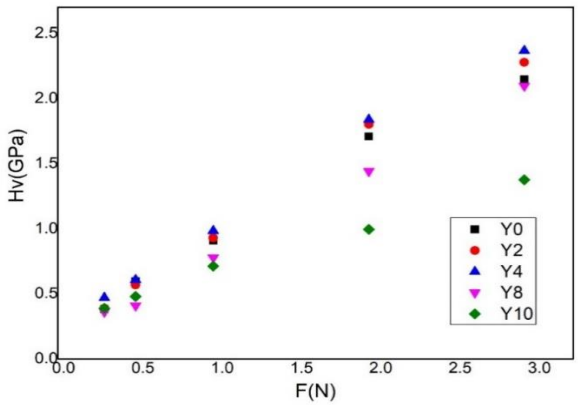

Figure 11. Variation of load dependent microhardness H_v of nano-Y doped samples with applied load F.

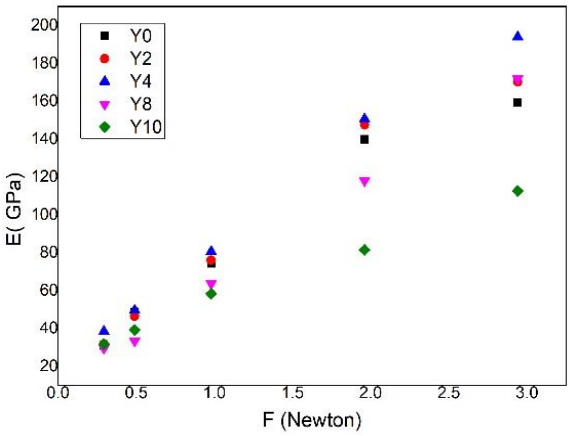

Figure 12. Variation of Young's modulus as a function of applied load

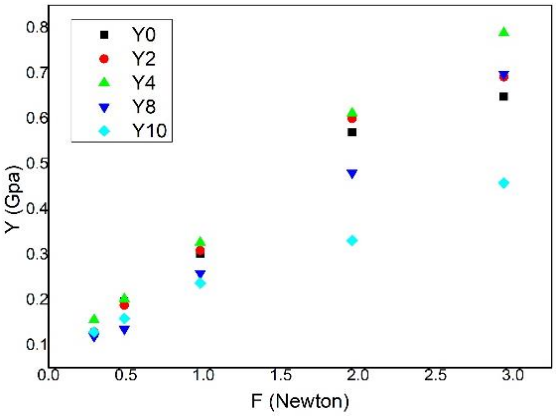

Figure 13. Variation of yield strength as a function of applied load

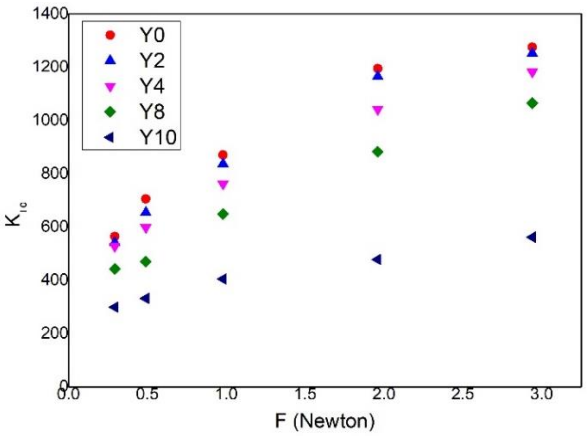

Figure 14. Variation of fracture toughness as a function of applied load

In **Figure 11**, The microhardness value increases non-linearly with the increasing applied force. Samples exhibiting this behavior, known as the reverse indentation size effect (RISE) in the literature, exhibit plastic deformation. The RISE behavior is a result of the bond strength between the superconducting grains and is caused by indentation-induced cracking [32]. Y4 sample has the highest hardness value. As supported by XRD results; compared to other nano-Y_2O_3 addition samples, the dislocation density of the Y4 sample is larger and the particle size is smaller. The dislocation density (δ) was calculated using the formula $\delta=1/D^2$ and calculated data are presented in **Table 2**. It is known that crystalline size and dislocation density vary inversely. As the δ value increases, the crystallinity level decreases [20]. Among all samples, the highest dislocation density belongs to Y2 and Y4 samples. The high hardness value is due to the high dislocation density [33]. Increased dislocation movement cause the tiny cracks to propagate rapidly. As the particle size gets smaller, the bond between the superconducting particles gets stronger and the mechanical strength is expected to increase. The hardness value of the doped samples decreased after x = 0.4 % additive value. We think that the decrease in microhardness with increasing additive content may be due to weakening of the bond between superconducting grains and randomly distributed irregularities at grain boundaries [34]. In the surface micrographs of samples **(Figure 5 a-e)** showed that grain sizes, porosity and surface cracks increase as Y-content increases.

Elastic modulus (E), yield strength (Y) and fracture toughness (K_{IC}) values of samples are presented in **Table 4.** Elastik modulus, an intrinsic property of the material, gives the relative stiffness of the material. Elastic modulus is a measure of resistance to elastic deformation. As the value of the elastic modulus decreases, elasticity of the material increases. In the case of an increase in elastic modulus, it means that elasticity of the material decreases [35]. Elastic modulus were calculated from Equation 6. Yield Strength, which is the magnitude of the stress at which a samples loses its elasticity and turns into plastic, is calculated from Equation 7. Also fracture toughness values of samples were calculated from Equation 8. 'Fracture toughness' describes the resistance of brittle materials to propagation of cracks under an applied force [36]. Fracture toughness, which is an important parameter in material selection in superconducting applications, is one of the main mechanical properties of superconducting samples.

$$E=81.9635H_v \quad (6)$$

$$Y\approx H_V/3 \quad (7)$$

$$K_{IC}=\sqrt{2E\gamma}(\gamma\ is\ energy\ surface) \quad (8)$$

Elastic modulus (E), yield strength (Y) and fracture toughness (K_{IC}) values increase with the increase in the applied load as seen in **Figure 11**, **Figure 12** and **Figure 13**. In addition, it is seen that E, Y and K_{IC} values increase up to x=0.4% additive value and decrease after x=0.4%.

It is seen in **Table 4** that hardness value increased until x = 0.4 % sample and decreased after this value. Especially the hardness value of Y10 sample is quite low compared to hardness values of all samples. When we add nano-Y_2O_3 at a certain rate, we see that the mechanical properties of the system are improved. After the amount of doping made after x= 0.4%, it affects the mechanical properties of the system negatively. We think that nano-dopings made in a certain amount can strengthen the interparticle connection by settling in the intergranular spaces. So we can say that nano-Y doping improves mechanical properties of BSCCO.

4. DISCUSSION AND CONCLUSION

In this study, $Bi_{1,8}Pb_{0,3}Sr_2Ca_2Cu_3O_y$ +$x(Y_2O_3)$ samples (where, x = 0.0, 0.2, 0.4, 0.8 and 1.0 wt %) were prepared by solid state reaction method. The effects of Y_2O_3 nanoparticles addition on the microstructure, phase formation, critical temperature, critical current density and microhardness values were investigated and compared by using XRD, SEM-EDX, Vibrating sample measurements and Microhardness measurements. The results obtained in this study on BSCCO superconducting are summarized as given below.

XRD measurement results showed that the volume fraction of Bi-2223 phase was the highest in undoped samples. Increasing the amount of nano-Y_2O_3 addition decreased volume fraction of 2223 phase, a small extent. No peaks belong to Y_2O_3 nanoparticles were found in the XRD pattern. This showed that Y_2O_3 nanoparticles cannot enter the structure. It is seen that a lattice parameter increased and c lattice parameter decreased with the increase in the amount of nano-Y_2O_3 addition. This indicated that the nano-Y_2O_3 addition affected the BSSCO crystal structure to a small extent. When we looked at the positions of the strongest peaks to belong to BSSCO, we did not see that there is no significant peak shift. Accordingly, we have seen that the orthorhombic structure continues to exist in all samples.

Table 4. The calculated load dependent H_v, E, Y and $K_{ıc}$ for Y0, Y2, Y4, Y8, and Y10 samples

Force (N)	Hv (Gpa)	E (Gpa)	Y (Gpa)	Kıc (Pa/m$^{1/2}$)
Y0				
0.294	0.380	31.21	0.126	564.20
0.49	0.595	48.79	0.198	705.51
0.98	0.906	74.31	0.302	870.61
1.961	1.707	139.95	0.569	1194.79
2.941	1.945	159.42	0.648	1275.20
Y2				
0.294	0.388	31.85	0.129	541.32
0.49	0.567	46.47	0.188	653.86
0.98	0.927	76.05	0.309	836.43
1.961	1.801	147.61	0.600	1165.37
2.941	2.076	170.18	0.692	1251.27
Y4				
0.294	0.470	38.52	0.156	526.65
0.49	0.606	49.66	0.202	598.02
0.98	0.983	80.57	0.327	761.64
1.961	1.838	150.64	0.612	1041.47
2.941	2.367	194.01	0.789	1181.88
Y8				
0.294	0.361	29.59	0.120	441.91
0.49	0.408	33.44	0.136	469.79
0.98	0.777	63.68	0.259	648.32
1.961	1.44	118.02	0.480	882.59
2.941	2.096	171.79	0.698	1064.82
Y10				
0.294	0.388	31.80	0.129	298.40
0.49	0.479	39.26	0.159	331.55
0.98	0.712	58.35	0.237	404.23
1.961	0.994	81.47	0.331	477.61
2.941	1.374	112.61	0.458	561.54

When the surface morphology of the samples was examined with SEM photographs, it was seen that the particle structure was plate-like. EDX analysis showed that there is no impurity formation in the materials and nano-Y_2O_3 addition are evenly distributed in the structure. When the M-H curves of the samples are examined, all samples showed diamagnetic properties.

The highest critical current density value for sample Y4 is 232 kA/cm^2. Except for the Y10 sample, the critical current density value of all samples is higher than the undoped sample. Nano-Y_2O_3 addition has a positive contribution to the formation of artificial needling centers. According to the results obtained from DC measurements, T_c^{onset} temperature values of Y2 and Y4 samples decrease slightly compared to the undoped sample. However, as the amount of additive increases, we see that the transition temperature to superconductivity decreases considerably. The hole concentration value ranges from 0.113 to 0.160. Hole concentration values of Y2 and Y4 samples are 0.16. Hole concentration values of Y8 and Y10 samples are 0.123 and 0.113, respectively. It is seen that the carrier density decreases after the value of nano-Y_2O_3 addition x=0.8 %. Vickers Microhardness measurement results showed that the microhardness value of the samples increases non-linearly with the increasing applied force. All samples exhibit RISE behavior. It is seen that the hardness values of the samples increase with increasing nano-Y_2O_3 addition.

Acknowledgement

We would like to thank Dokuz Eylül University faculty member Dr. Özlem Bilgili and İzmir University of Economics Faculty Member Hasan Durmuş for their valuable advice.

REFERENCES

[1] Kim CJ. Superconductor Levitation Concepts and Experiments (e Book). Springer Nature; 2019. https://doi.org/10.1007/978-981-13-6768-7

[2] Abou-Aly A, Abdel Gawad MMH, Awad R, G-Eldeen I. Improving the Physical Properties of (Bi, Pb)-2223 Phase by SnO2 Nano-particles Addition. J. Supercond. Nov. Magn.2011; 24, (7): 2077-84.

[3] Awad R. Study of the Influence of MgO Nano-Oxide Addition on the Electrical and Mechanical Properties of (Cu0.25Tl0.75)-1234 Superconducting Phase. J Supercond. Nov. Magn. 2008; 21: 461–6

[4] Öztornacı U, Özkurt B. The effect of nano-sized metallic Au addition on structural and magnetic properties of Bi1.8Sr2 AuxCa1.1Cu2.1Oy (Bi-2212) ceramics. Ceram. İnter. 2017; 43 (5): 4545-50.

[5] Mawassi R, Marhaba S, Roumié M Awad R, Korek M, Hassan I. Improvement of Superconducting Parameters of Bi 1.8Pb0.4Sr2Ca2Cu3O10+δ Added with Nano-Ag. J. Supercond. Nov. Magn. 2014; 27:1131–42.

[6] Yahya NAA, Al-Gaashani R, Abd-Shukor R. Synthesis and characterization of PbO–CdO nanocomposite and its effect on (Bi,Pb)-2223 superconductor. Appl. Phys. A. 2017;123-68.

[7] Jia ZY, Tang H, Yang ZQ, Xing YT, Wang YZ, Qiao GW. Effects of nano-ZrO particles on the

superconductivity of Pb-doped BSCCO. Phys. C. 2000; 337:130–2.

[8] Yıldırım G, Dogruer M, Karaboga F, Terzioglu C. Formation of nucleation centers for vortices in Bi-2223 superconducting core by dispersed Sn nanoparticles. J. All. Comp. 2014; 584: 344-51.

[9] Mohammed LA, Jasim KA. The substitutions of Strontium by yttrium and their effects on Bi2Sr2-xYxCa2Cu3O10+δ superconducting compound. Journal of Physics: Conference Series. 2021. 1879 (032069)

[10] Dong Y, Sun A, Xu B, Zhang H, Zhang M. Effect of the BSCCO superconducting properties by tiny Y2O3 addition. Mod. Phys. Let. B. 2016; 30 (26): 1650328/1-9.

[11] Khalil SM. Effect of Y3+ substitution for Ca on the transport and mechanical properties of Bi2Sr2Ca1−xYxCu2O8+δ system. J. Phys. Chem. Sol. 2003; 64 (5): 855-61.

[12] Sedky A. The impact of Y substitution on the 110 K high Tc phase in Bi (Pb):2223 superconductor. J. Phys. Chem. Sol. 2009;70: 483-88.

[13] Suazlina MA, Yusainee SYS, Azhan H, Abd-Shukor R, Mustaqim R. The Effects of Nanoparticle Addition in Bi-2212 Superconductors. 2014; 69 (2): 49–52.

[14] Oboudi SF. Synthesis and Magnetic Properties of Bi1.7Pb 0.3Sr2Ca2Cu3O10+δ Added with Nano Y. J. Supercond. Nov. Magn. 2017; 30: 1473–82.

[15] Durmus H, Kocabas K. The influence of Mn nanoparticles on superconducting properties and pinning mechanism of MgB2. J. Mater. Sci. Mater. Electr. 33 (21): 17079–89.

[16] Çorduk T, Bilgili O, Kemal K. Investigation of effects of MgO nanoparticles addition on the superconducting properties of Bi-2223 superconductors. J. Mater. Sci. Mater. Electr. 2017; 28 (11): 14689–95.

[17] Cevizci B, Bilgili O, Kemal K. The influence of Ag substitution on structural and mechanical properties of (Bi, Pb)-2223 ceramics. J.Mater. Sci. Mater. Elect. 2016; 27 (12), 13171-78.

[18] Bilgili O, Yurdaskal M. Effects of Graphene Oxide Doping on Magnetic and Structural Properties of Bi1.6Pb0.4Sr2Ca2Cu3Oy Superconductor. J.Elect. Mat.2021; 50: 4999–5006.

[19] Yildirim G, Dogruer M, Karaboga F, Terzioglu C. Formation of nucleation centers for vortices in Bi-2223 superconducting core by dispersed Sn nanoparticles. J. All. Comp.2014; 584: 344–51.

[20] Bilgili O. Structural and Electrical Properties of Nanosized Sm2O3 Doped Bi1.6Pb0.4Sr2Ca2Cu3Oy Superconductors .J. Low. Temp. Phys.2021; 204: 5-6.

[21] Shamray VF, Mikhailova AB, Mitin AV. Crystal structure and superconductivity of Bi-2223. Cryst Rep.2009; 54: 584–590.

[22] Scherrer P. Nachrichten von der Gesellschaft der Wissenschaften zu Göttingen. Mat. Phys. Klas. 1918; 2: 98-100.

[23] Langford J I, Wilson A J C Scherrer after Sixty Years: A Survey and Some New Results in the Determination of Crystallite Size. J. Appl. Cryst.1978; 11: 102-113.

[24] Abou-Aly A I, Abdel Gawad M M H, Awad R, G-Eldeen I. Improving the Physical Properties of (Bi, Pb)-2223 Phase by SnO2 Nano-particles Addition. J. Supercond. Nov. Magn. 2011; 24: 2077–84.

[25] Bean CP. Magnetization Of Hard Superconductors. Phys. Rev. Lett. 1962; 8 (6): 250-3.

[26] Yahya NAA, Abd-Shukor R. Effect of Different Nanosized MgO on the Transport Critical Current Density of Bi1.6Pb0.4Sr2Ca2Cu3O10 Superconductor. J. Supercond. Nov. Magn. 2014; 27: 329-35.

[27] Turk N, Gundogmus H, Akyol M, Yakıncı D, Ekicibil A, Ozcelik B. Effect of Tungsten (W) Substitution on the Physical Properties of Bi-(2223) Superconductors. J. Supercond. Nov. Magn. 2014; 27: 711–16.

[28] Persland M R, Tallon J L, Buckley R G, Liu R S, Floer N E. General trends in oxygen stoichiometry effects on Tc in Bi and Tl superconductors. Phys. C. 1191; 176 (1–3): 95–105.

[29] Bilgili O, Selamet Y, Kocabas K. Effects of Li Substitution in Bi-2223 Superconductors. J. Supercond. Nov. Magn. 2008; 21: 439–49.

[30] Saritekin N K, Tutuncu A T. Improving Superconductivity, Microstructure, and Mechanical Properties by Substituting Different Ionic Pb Elements to Bi and Ca Elements in Bi 2223 Superconductors. J. Supercond. Nov. Magn. 2022; 35: 2259–73.

[31] Uvarov V, Popov I. Metrological characterization of X-ray diffraction methods at different acquisition geometries for determination of crystallite size in nano-scale materials. Mater. Charac.2013; 85: 111-123.

[32] Safran S, Ozturk H, Bulut F, Ozturk O. The influence of re-pelletization and heat treatment on physical, superconducting, magnetic and micro-mechanical properties of bulk BSCCO samples prepared by ammonium nitrate precipitation method. Ceram. Inter. 2017; 43: 15586–92.

[33] Li H, Bradt R C. The effect of indentation-induced cracking on the apparent microhardness. J.Mat. Sci. 1966; 31: 1065-70.

[34] Ozturk O, Asikuzun E, Tasci A T, Gokcen T, Ada H, Koralay H, Cavdar S. Comparison of Vickers microhardness of undoped and Ru doped BSCCO glass ceramic materials. J.Mater. Sci. Mater. Elect. 2018; 29: 3957–66.

[35] Jones DRH, Ashby MF. Engineering Materials 1: An Introduction to Properties, Applications and Design. Chapter 3 - The Elastic Moduli. 5 th ed. Elsevier Science press; 2019. p.29-53.

[36] Jones DRH, Ashby MF. Engineering Materials 1: An Introduction to Properties, Applications and Design. Chapter 8 - Yield Strength, Tensile Strength, and Ductility. 5 th ed. Elsevier Science press; 2019. p.115-133.